The DOI for this manuscript is doi: 10.1175/JCLI-D-18-0305.1

The final published version of this manuscript will replace the preliminary version at the above DOI once it is available.

If you would like to cite this EOR in a separate work, please use the following full citation:

Feng, J., J. Li, F. Kucharski, Y. Wang, C. Sun, F. Xie, and Y. Yang, 2018: Modulation of the meridional structures of the Indo-Pacific warm pool on the response of the Hadley circulation to tropical SST. J. Climate. doi:10.1175/JCLI-D-18-0305.1, in press.

Modulation of the meridional structures of the Indo-Pacific warm pool on the response of the Hadley circulation to tropical SST

Juan Feng[1], Jianping Li[1,2], Fred Kucharski[3, 4], Yaqi Wang[1], Cheng Sun[1], Fei Xie[1], and Yun Yang[1]

1. College of Global Change and Earth System Science, Beijing Normal University, Beijing, 100875, China

2. Laboratory for Regional Oceanography and Numerical Modeling, Qingdao National Laboratory for Marine Science and Technology, Qingdao, China

3. Earth System Physics Section, Abdus Salam International Centre for Theoretical Physics, Trieste 34151, Italy

4. Department of Meteorology, Center of Excellence for Climate Change Research, King Abdulaziz University, Jeddah, Saudi Arabia

***Corresponding author*:**

Dr. Juan Feng

College of Global Change and Earth System Science (GCESS)

Beijing Normal University, Beijing, China

Email: fengjuan@bnu.edu.cn

Abstract

By decomposing the variations of the Hadley circulation (HC) and tropical zonal mean sea surface temperature (SST) into the equatorially asymmetric (HEA for HC, SEA for SST) and symmetric (HES for HC, SES for SST) components, the varying response of the HC to different SST meridional structures under warm and cold conditions of the Indo-Pacific warm pool (IPWP) is investigated over the period 1979–2016. The response of the HC to SST evidences an asymmetric variation between warm and cold IPWP conditions; i.e., the response ratio of HEA to SEA relative to that of HES to SES is ~5 under warm conditions and ~2 under cold conditions. This asymmetry is primarily due to a decrease in the HEA to SEA ratio under cold IPWP conditions, and is driven by changes in the meridional distribution of SST anomalies. Equatorial asymmetric (symmetric) SST anomalies are dominated with warm (cold) IPWP conditions. Thus, variations of SEA are suppressed under cold IPWP conditions, contributing to the observed weakening of the HEA to SEA ratio. Results presented here indicate that the HC is more sensitive to underlying SST when the IPWP is warmer during which the variation of SEA is enhanced, suggesting a recent strengthening of the response of the HC to SST as the IPWP has warmed over the past several decades, and highlighting the importance of the IPWP meridional structures rather than overall warming on the HC.

1. Introduction

The Indo-Pacific warm pool (IPWP) is the largest warm water mass in the world, where the sea surface temperature (SST) exceeds 28°C year-round (Yan et al. 1992). The IPWP plays an important role in the atmospheric circulation system by releasing its energy to the atmosphere in the form of heat and water vapor, leading to an extremely strong air–sea interaction in this region (Xie et al. 2005; Duan et al. 2008). Globally, the IPWP is one of the major suppliers of atmospheric heat and water vapor, and also undergoes the most intense global air convection, making this area an important source of global climate anomalies (Li et al. 2013). The importance of the IPWP in the evolution of atmospheric circulation is summarized by the following two observations. First, changes in SST in the IPWP, particularly for high SST, affect the convergence of the atmosphere. The resulting divergence and vertical motion have a great influence on the global climate, and may directly affect the Hadley circulation (HC) and Walker circulation (Sardeshmukh and Hoskins 1988; Webster and Lukas 1992). Secondly, because the IPWP is the most frequently convective area in the world, convection changes in the IPWP can trigger a series of global and regional climate phenomena (Feng et al. 2013; Li et al. 2013). Therefore, variations of SST in the IPWP play a fundamental role in the formation of global climate anomalies and disasters (e.g., Williams and Funk 2011; Luo et al. 2012; Lo et al. 2014).

The HC is a thermally driven meridional circulation, and is one of the most important and largest circulation systems on the planet. In the vertical direction, the HC features an ascending branch in the tropics combined with two descending branches located in the subtropical regions of both hemispheres. In the horizontal direction, the HC is characterized by poleward mass transport in the upper troposphere and equatorward mass transport by the prevailing trade winds in the lower troposphere (Quan et al. 2004). Thus, the HC bridges the lower and upper troposphere, as well as the tropics and subtropics. A change in either its spatial structure or intensity can have great climatic effects. Therefore, it has frequently been reported that the HC plays an important role in climate processes at low, mid, and high latitudes (e.g., Lindzen 1994; Chang 1995; Diaz and Bradley 2004; Feng et al. 2013).

Over the past 60 years, observations have shown that the IPWP has been warming and expanding, particularly in recent decades (e.g., Alory et al. 2007; Rao et al. 2012; Dong et al. 2014; Kidwell et al. 2015). Several studies have investigated the possible causes and climatic effects of this warming. It has been suggested that the observed warming is connected to the increasing frequency of El Niño events (e.g., Cai et al. 2014), that both air and ocean processes participate in IPWP warming (Rao et al. 2012; Swapna et al. 2014), and that both anthropogenic and natural forcing contribute to IPWP warming (e.g., Dong et al. 2014; Roxy et al. 2014). Although the cause of the continuous warming of the IPWP remains ambiguous, these studies have confirmed that the IPWP has been continuously warming over the past 60 years. Given that the HC is a thermally driven circulation, it is strongly influenced by underlying thermal condition in the tropics. The potential influence of IPWP warming on the HC has been explored. It was found that IPWP warming contributed to a strengthening of the first dominant mode of the long-term variability of the seasonal HC (e.g., Ma and Li 2008; Feng et al. 2011; Feng et al. 2013). Moreover, inhomogeneous warming within the IPWP (i.e., a relatively higher warming rate in the southern IPWP) could alter the SST meridional gradient, which could in turn affect the formation of the dominant mode of the seasonal HC (Feng et al. 2013; Li and Feng 2017). This research highlights the important role of the IPWP, particularly the warming of the IPWP, on variations in the HC.

The HC depends not only on the intensity of the underlying thermal conditions, but also on the meridional distribution of the underlying SSTs. Earlier theoretical works have established that the meridional structure of tropical SST determines the position and intensity of the convergence (e.g., Schneider and Lindzen 1977; Rind and Rossow 1984; Lindzen and Nigram 1987). Our recent studies have demonstrated that equatorially asymmetric (symmetric) meridional circulation are associated with an equatorially asymmetric (symmetric) SST anomalies based on observational datasets and numerical experiments (Feng et al. 2013; Feng and Li 2013). Moreover, we found that the magnitude of the anomalous HC response to the equatorially asymmetric SST is ~4 times greater than that to the equatorially symmetric SST even if the intensity of the SST is the same in both the interannual and annual cycles (Feng et al. 2016a; Feng et al. 2017). The above findings highlight the importance of the meridional distributions of tropical SST to the response of the HC to the SST.

Although the IPWP shows a strong warming trend and plays an important role in the variability of the HC, it is still unknown whether IPWP warming plays a role in the response of the HC to SST, and if so, what mechanisms are involved. Thus, the focus of this work is to investigate the impact of the warm and cold IPWP situations on the sensitivity of the HC to different SST meridional structures, while Feng et al. (2016) only focused on the response of the HC to SST without examining the modulation of the IPWP intensity. The remainder of this paper is organized as follows. Section 2 describes the datasets and methodology. The influence of the IPWP on the HC response to SST is presented in section 3. A possible mechanism for this influence is described in section 4. Finally, section 5 contains a discussion and conclusions.

2. Datasets and methodology

2.1 Datasets

Four atmospheric reanalysis datasets were employed to objectively evaluate the characteristics of the HC. These datasets were from the Japanese 55-year Reanalysis (JRA) on a horizontal resolution of 1.25°×1.25° and 32 vertical levels (Kobayashi et al. 2015), the National Centers for Environmental Prediction-Department of Energy Atmospheric Model Intercomparison Project reanalysis (NCEP2) covering the period 1979 to 2016 on 17 vertical levels (Kanamitsu et al. 2002), the European Centre for Medium-Range Weather Forecasts (ECMWF) Re-Analysis interim (ERAI) globally archived dataset that covers 1979 to 2016 with a resolution of 1.5° × 1.5° on 32 vertical levels (Dee et al. 2011), and the ERA-40 reanalysis data on a horizontal resolution of 2.5°×2.5° and 18 vertical levels (Uppala et al. 2005). Two global SST reanalysis datasets are used to examine the tropical SST features as a comparison to verify the reliability of the results. They are the UK Met Office Hadley Centre's sea ice and SST dataset with a 1°×1° horizontal resolution (HadISST; Rayner et al. 2003), and the Extended Reconstructed SST version 3 (ERSST) on a 2°×2° resolution (Smith et al. 2008). The common available period of 1979–2016 based on the NCEP2 and JRA was used to illustrate the interannual influences of the IPWP on the response of the HC to tropical SST. And the period 1958-2001 based on the ERA40 was employed to outline the interdecadal influence of the IPWP on the response of the HC to SST.

2.2 Method

The HC is characterized by the mass stream-function (MSF). The detailed calculation of the MSF is seen in Feng et al. (2016a). To evaluate the impacts of the IPWP on the response of the HC to different SST meridional structures, the variations of the MSF and zonal mean SST are decomposed into two components, i.e., the equatorially symmetric and asymmetric variations, based on the linearly decomposition method according to Feng et al. (2017). The symmetric and asymmetric components of zonal mean SST (referred as SES and SEA in the context) is obtained as follows,

$$SES(y) = \frac{SST(y) + SST(-y)}{2}, \quad SEA(y) = \frac{SST(y) - SST(-y)}{2} \qquad (1)$$

The equatorially asymmetric and symmetric variations of MSF is defined as follows,

$$HEA(y) = \frac{MSF(y) + MSF(-y)}{2}, \quad HES(y) = \frac{MSF(y) - MSF(-y)}{2}, \qquad (2)$$

where y is the meridional location north of the equator. Note that the MSF is a two dimension variable without x direction. To this point, the distribution of land-sea would not contaminate the calculation of the MSF, either the decomposition. The detailed illustration and calculation of the above decomposition are displayed in Feng et al. (2017). The relative response amplitude of the HC to different SST meridional structures is considered according to the definition of response ratio,

$$ratio = \frac{\mathrm{Reg}(\mathrm{PC1(HEA)}, \mathrm{PC1(SEA)})}{\mathrm{Reg}(\mathrm{PC1(HES)}, \mathrm{PC1(SES)})} \quad (3)$$

where PC1(HEA) refers to the first principal components (PC) of the variability of HEA, the other variables refer similar meanings. The numerator (denominator) in equation (3) depicts the response amplitude of the HEA (HES) to the SEA (SES) by regressing the HEA PC1 with respect to the SEA PC1. To this point, the variable *ratio* depicts the relative change in the HC response to SST. Even if different reanalyses are used, the possible impacts of the different assimilation systems would be counterpart for both the numerator and denominator contain the variables of circulation and SST.

To demonstrate the difference in the response of the HC to SST between warm and cold events, the areal averaged SST anomalies within the IPWP (IPWPI) is taken as an index to select the warm and cold events. Here, the scope 40°-160°E, 20°S-20°N is taken as the extent to identify the features of the IPWP. This is due to the following three considerations, 1) this region includes the main body of the warm pool (figure not shown); 2) to distinguish the possible influence from the central Pacific, as could be seen below that SST anomalies during the warm and cold IPWP conditions are different in the central Pacific. 3) The areal averaged monthly SST over other IPWP extent (i.e., 10°S-20°N, 60°-180°E) is highly correlated with the IPWPI, with a correlation coefficient of 0.6 (with a length of 456 month), indicating the chosen extent depicts the main characteristics of the SST over the IPWP. The calendar year is used to depict a cycle of IPWP event, in which the monthly IPWPI above (below) 1 (-1) standard deviation for at least 6 months is defined as a warm (cold) IPWP year. This gives six warm events (i.e., 1981, 1988, 1998, 2003, 2010, and 2016) and six cold events (i.e., 1986, 1992, 1993, 1994, 2006, and 2008) during the period 1979–2016. A same definition of the warm and cold IPWP events but based on the domain (i.e., 10°S-20°N, 60°-180°E) would give four warm (1988, 1998, 2003, and 2016) and cold (1992, 1993, 1994, and 2008) events. The four warm and cold events are coincided with the warm and cold events based on the 20°S-20°N, 40°-160°E. And it is found that the ratio of the HC to SST during the warm and cold events of the IPWP based on the four events is consistent with the result shown in the context, indicating the result shown is not subjected to the selection of IPWP domain.

In addition, it is noted that five (i.e., 1988, 1998, 2003, 2010, and 2016) of the six warm events are coincided with the decaying phase of El Niño events, whereas only two cold event (2006 and 2008) are coincided with the decaying phase of La Niña event, indicating important role of El Niño on the SST over IPWP as suggested in previous studies (Lau and Nath 2003; Xie et al. 2009; Santoso et al. 2017). In addition, it is seen that the asymmetric influences of the El Niño and La Niña on the SST over the IPWP, for that five of the six warm IPWP events coincide with the occurrence of El Niño, while only two cold IPWP events coincide with La Niña event. Three of the cold events (i.e., 1992, 1993, and 1994) are following the 1991 Pinatubo eruption, which is the second largest eruption in the 20^{th} century, resulting a global scale cooling after several years following the eruption (Xiao and Li 2011; Zhang et al. 2018). These six warm and six cold events constitute the subsets of warm and cold events with lengths of 72 (6 events ×12 month a year) months, and the 38 calendar years (i.e., from 1979 to 2016) constitute the whole study period with a length of 456 (38×12) months in the following analysis. It should be noted is that the warm (cold) IPWP events are discontinuous in time; the annual cycle and linear trend before constructing the warm and cold subsets have been removed to reduce the possible influences of the discontinuity and continuously warming of the IPWP (figures not shown). The climatology to construct the anomalies is referenced to the entire 38 years, as well as the linear trend.

Empirical orthogonal function (EOF) analysis was used to detect the dominant mode of the HC and monthly zonal mean SST during the warm (cold) IPWP events. Composite analysis was used to compare the associated SST anomalies associated with the warm and cold IPWP conditions. To investigate the source of the differences between the warm and cold IPWP events, instead of the commonly used composite method, we calculated the sum of the anomalies during the warm and cold events (both are with a length of 72 months) to highlight the possible origin of their associated distinctions. Correlation and regression analyses were employed to investigate the relationship between the HC and SST. The statistical significance of the correlation, regression and composite values were evaluated by means of a two-sided Student's *t*-test.

3. Interannual influence of the IPWP on the HC response to SST

a) Variations in the HEA and HES

The equatorially asymmetric and symmetric HC variations were obtained according to the above decomposition. Figure 1 shows the climatology and the first EOF mode (EOF1) of the HEA and HES during warm IPWP events over the period 1979–2016. Because the decomposition of the asymmetric and symmetric components is based on the position of the equator, the value of HES at the equator is always zero. The JRA, NCEP2, and EARI datasets were used to validate the reliability of the dominant modes of HEA and HES interannual variability. The climatological HEA based on the three reanalyses both have a similar structure, with ascending motion to the north of the equator, and descending motion to the south of the equator. The climatological HES based on the three reanalyses have a consistent structure, with two comparable cells on the flanks of the equator, showing a common ascent over the equatorial belt and descent over the subtropics in each hemisphere (Feng et al. 2016a). The extents of the climatological HEA and HES are comparable, but the intensity of the HES is greater than that of the HEA. The EOF1 of the HEA has a similar spatial structure, but the extent is narrower compared with its climatology, with ascending motion around 10°N, and descending motion around

10°S. The EOF1 of HEA accounts for ~50% of the total variance, being more concentrated than that during the entire study period (~30%; figures not shown). The spatial distribution of the HES EOF1 follows its climatological structure, accounting for ~40% of the total variance. The spatial structures and explained variance of the dominant modes for both the HEA and HES are in good agreement across the three reanalyses, indicating the reliability of the results. As to the intensity of the EOF1, since the EOF is based on the anomalies, the spatial distribution of the EOF modes as well as its corresponding PCs should be considered together to depict the magnitude of the EOF modes. It is seen the amplitude of the HEA (HES) PC1s based on NCEP2 is about 2 times to that based on JRA and ERAI (figures not shown). That is the variability of the corresponding EOF modes is comparable across the three reanalyses.

The EOF1 of HEA and HES during cold IPWP events is shown in Figure 2. The climatology distribution of the HEA and HES during cold IPWP events is similar to those during warm events. However, compared with the case during warm IPWP events, a broader HEA EOF1 extent with a smaller explained variance are observed for all the reanalyses. However, the intensity and the explained variance of the HES EOF1 are similar to those of warm IPWP events, with a broader extent during the cold events. These results imply that the variability of the HEA is more sensitive to IPWP thermal conditions than is that of the HES; i.e., cold IPWP conditions may suppress the variation of the HEA, but not that of the HES.

b) Variations in the SEA and SES

Figure 3 displays the principal mode of the SEA and SES during warm and cold events based on the ERSST and HadISST datasets, respectively. The two reanalyses are consistent in their spatial distributions. The EOF1 of SEA indicates a sinusoidal variation, with positive values in the Northern Hemisphere (NH), and negative values in the Southern Hemisphere (SH) during both warm and cold events. Note that the EOF1 during warm events has a maximum (minimum) around 10°N (10°S), corresponding to the locations where the meridional gradient of SST changes from positive (negative) to negative (positive), and parallel to the location of the ascending (descending) branch of the HC according to the relation of meridional wind and SST described in Feng and Li (2013). The deduction here is consistent with the ascending and descending positions shown in Figure 1. However, the spatial distribution of the SEA EOF1 during cold events is much flatter and lacks an evident peak in the range 20°S–20°N, favoring a broader HC, as shown in Figure 2. However, uncertainties exist in the explained variance of this mode; i.e., enhanced explained variance during cold IPWP events is seen for ERSST, while the opposite is observed for HadISST.

The EOF1 of the SES exhibits a parabolic-like variation centered at the equator during both the warm and cold IPWP events. Note that the peak value at the equator during the cold IPWP events is larger than that during the warm events, indicating a broader meridional circulation (Feng et al. 2013; Feng and Li 2013), explaining why the extent of the HES EOF1 is broader during cold IPWP events. The explained variance of the SES EOF1 is consistently enhanced during warm events compared with that during cold events in both ERSST and HadISST datasets, consistent with the association of El Niño events with equatorial symmetric SST anomalies within the tropics (Cane and Zebiak 1985). It should be noted that five of the six warm events coincided with El Niño events. Thus, the SES component is enhanced during warm IPWP events, leading to the decreased explained variance of the SES EOF1 during cold IPWP events.

c) Response ratio of the HC to SST

The above results demonstrate that both the spatial distributions and the explained variance of the dominant modes of HEA and HES, as well as SEA and SES, undergo certain changes between warm and cold IPWP events, regardless of whether the HC response amplitudes to different SST meridional structures in the two situations differ. Figure 4 presents scatterplots of the PC1 of SEA against HEA, and of SES against HES during the warm and cold IPWP events, based on ERSST and JRA datasets. The NCEP2 and HadISST datasets led to similar results (not shown; Table 1). The variation of HEA (HES) is significantly linearly correlated with SEA (SES). Moreover, the response coefficient of HEA to SEA is largely suppressed during cold IPWP events; i.e., a 1-unit change in SEA is associated with an 83-unit change in the HEA during warm events, but with a 29-unit change during cold events. However, the response coefficients of HES to SES undergo little change; i.e., a 1-unit change in SES is associated with a 14-unit change in HES during both warm and cold IPWP events. This result is consistent across the different reanalyses, as shown in Table 1, suggesting that the response of HEA to SEA is largely suppressed during cold IPWP events. Thus, the response contrast of the HC to different SST meridional structures is distinct between the warm and cold IPWP events; i.e., it is about 5 during warm events among the different reanalyses, whereas it is about 2 during cold IPWP events (Table 1). The response contrast of the HC to SST during warm events is equivalent to that of the long-term interannual variation in the seasonal cycle, as previously reported (Feng et al. 2016a; Feng et al. 2017). These results imply that the HC is not as sensitive to underlying thermal conditions during cold IPWP events as it is during warm events.

The above results indicate that the HC response to different SST meridional structures varies with thermal conditions. The suppressed response contrast of the HC to SST is primarily due to the suppressed response of equatorially asymmetric variations. Potential causes for the suppressed influence of equatorially asymmetric variations will be discussed in the following section.

4. Possible mechanisms for the varied ratio

To explore potential mechanisms for the suppressed response contrast of the HC to different SST meridional structures under cold IPWP conditions, we first examined the associated anomalous SST patterns under warm and cold IPWP conditions (Figure 5). Warm IPWP conditions are accompanied by significant positive SST anomalies over the IPWP, tropical Atlantic, and southeastern Australian coastal regions (Figure 5a). Negative SST anomalies are seen over the tropical eastern and central Pacific during warm events. In contrast, an insignificant El Niño-like pattern is observed during cold events, with no significant positive SST anomalies in the eastern and central Pacific, but with significant negative SST anomalies over the IPWP (Figure 5b). A comparison between warm and cold conditions reveals the following distinct differences. First, the magnitude of SST anomalies under warm and cold IPWP conditions is not equivalent, particularly within the IPWP. The equatorial flanks of the IPWP are associated with positive SST anomalies in general (Figure 5c), indicating the magnitude of SST anomalies associated with warm IPWP conditions is greater than that under cold conditions. Secondly, the magnitude of the warming in the southern IPWP is greater than that in the northern IPWP, indicating an inhomogeneous change occurs across the northern and southern IPWP, which in turn would induce an anomalous meridional gradient of SST within the IPWP. This is further verified by the zonal mean SST profiles within the IPWP domain (Figure 6). Under warm IPWP conditions, the magnitude of warming in the southern IPWP is greater than in its northern counterpart. The maximum warming occurs around 10°S, and the minimum occurs near the equator. The convergence in the lower troposphere is subject to the meridional gradient of SST (Feng et al. 2013; Feng and Li 2013), indicating an anomalous equatorially asymmetric meridional circulation associated with this anomalous SST distribution. The anomalous equatorially asymmetric circulation favors an intensified equatorially asymmetric component of the HC, contributing to the enhanced explained variance of the HEA EOF1 compared with that in the entire period. For that the EOF1 explains ~30% of the variance for the HEA across the three reanalyses during the entire study period, whereas it is around 50% during the warm IPWP events. However, the zonal mean SST profile under cold

IPWP conditions is equatorially symmetric in general, with the maximum at the equator. Therefore, an equatorially symmetric anomalous meridional circulation would be associated with this type of SST anomaly. The associated anomalous circulation would counterbalance the equatorially asymmetric variation of the meridional circulation, leading to a suppressed explained variance for HEA EOF1 under cold IPWP conditions, as described in section 3 (Figure 1 vs. Figure 2), and contributing to the suppressed response contrast of the HC to SST. Different meridional distributions of SST anomalies under warm and cold IPWP conditions provide a potential explanation for the suppressed response of the HC to SST during cold events. This is further verified by the sum of the warm and cold IPWP conditions, which supports this potential source of the differences between the warm and cold events. An evident equatorially asymmetric SST distribution is seen in the sum of the warm and cold IPWP events, with the maximum around 10°S and the minimum around 10°N (Figure 6c). To further verify the role of this SST anomaly on the meridional circulation, a meridional SST gradient index (MSGI) within the IPWP is defined as follows:

$$MSGI = SST_{[0°\text{–}20N°,\ 40°E\text{–}160°E]} - SST_{[20S°\text{–}0°,\ 40°E\text{–}160°E]}. \quad (4)$$

The relationship between the IPWPI and MSGI is not significant, with a correlation coefficient of -0.05. The influence of the anomalous SST meridional gradient within the IPWP on the meridional circulation was further established by determining the regressions between the MSGI and the meridional circulation in terms of the MSF and zonal mean vertical motion (Figure 7). The regression pattern indicates an equatorially asymmetric circulation, with ascent located around 10°N, and descent around 10°S, which is consistently observed in both the vertical motion (contours) and MSF (shaded). This indicates that the meridional circulation connected with the MSGI is equatorially asymmetric. Moreover, we note that the meridional distribution in the sum of the warm and cold events is similar to the distribution during warm events, suggesting the difference between the warm and cold events is mainly driven by the warm events.

In addition, there are significant negative SST anomalies over the north Pacific (30°–50°N, 140°E–130°W) during warm IPWP events, but no significant signal during cold IPWP events (Figure 5). The difference between the warm and cold IPWP events in the north Pacific is further seen in the sum of the warm and cold events (Figure 5c). We examined the SST variation over this region, and found that the evolution of SST over the north Pacific undergoes a varying seasonal evolution (Figure 8). Results from two SST reanalyses indicate that the amplitude of SST anomalies over the north Pacific are larger during warm IPWP events, and that there are negative SST anomalies year-round during warm IPWP events. The area-averaged SST over the north Pacific was employed to further investigate its possible influence on the meridional circulation (figure not shown). However, the associated meridional circulation is not significant in either the vertical motion or in the MSF, suggesting the influence of SST over the north Pacific on the HC is limited.

The results presented above suggest that the difference in the response ratio of the HC to different SST meridional structures is primarily due to the associated SST anomalies within the IPWP; i.e., different SST meridional distributions are associated with warm and cold IPWP conditions. Warm IPWP conditions are associated with an inhomogeneous meridional distribution, with greater amplitude in the southern IPWP, which induce an equatorially asymmetric circulation. Conversely, the meridional distribution of SST is equatorially symmetric during the cold IPWP conditions, suppressing the variation of the equatorially asymmetric component of the HC.

5. Discussion and summary

Using recent 38-year reanalysis data sets, we investigated the influence of the IPWP on the response contrast of the HC to different SST meridional structures by detecting the response characteristics of the HC to SST under warm and cold IPWP conditions. It was found that the response contrast of the HC to different SST meridional structures differs between warm and cold IPWP conditions. The response contrast of HC to SST during warm IPWP events is comparable to that of the long term and seasonal cycles, as previously reported. However, it is generally suppressed under cold IPWP conditions. This result implies that the HC is more sensitive to the underlying thermal structures when the IPWP is warmer. Because the IPWP has been warming over the past 60 years (Rao et al. 2012; Feng et al. 2013), the results of this study suggest that the response ratio of the HC to tropical SST may have been recently enhanced, particularly as it relates to equatorially asymmetric variations under the influence of the continuous IPWP warming. And it is highlighted that it is the meridional structures plays important role in impacting the response of the HC to SST rather than the overall warming conditions.

A potential cause of the suppressed response of the HC to SST during cold IPWP events was also explored. It was found that the meridional distribution of SST anomalies within the IPWP under cold conditions is equatorially symmetric, in general. However, this was not the case for warm IPWP events, during which a larger amplitude in the southern IPWP was observed. Moreover, the distinction between warm and cold SST events were primarily located in the IPWP, with similar spatial distributions to those displayed during warm IPWP events. However, the sum differences of the warm and cold IPWP events were accompanied by an equatorially asymmetric meridional circulation, favorable for the intensification of the HEA EOF1. These results highlight the importance of differences in the meridional distributions of anomalous SST within the IPWP between warm and cold IPWP events to the response contrast of the HC to SST. In addition, another significant difference between the warm and cold IPWP events was found in the north Pacific; however, it suggests that the relationship between SST over the north Pacific and the HC is insignificant. It is thus concluded that differences in the response of the HC to SST between warm and cold IPWP events is primarily due to differences in SST meridional anomalies within the IPWP. Besides, significant signal over the tropical Atlantic is also observed (Figure 5), however, is not as extensive as the IPWP, the possible influences of the tropical Atlantic oceans on the response of the HC to SST warrant further work.

As reported in previous studies, El Niño events have important impacts on SST over the IPWP. It is unknown whether results presented here were contaminated by El Niño effects. We further detected the impacts of the IPWP on the response of the HC to SST by employing long-term datasets. Because the IPWP has undergone continuous warming, and a long period analysis may be influenced by this linear trend, we selected two sub-periods, 1958–1972 and 1987–2001, as the cold and warm phases of the IPWP, respectively, and compared the response of the HC to SST between the two sub-periods. Here, the two sub-periods were selected based on the availability of ERA40 reanalysis data, because the National Centers for Environment Prediction/National Center for Atmospheric Research is limited in its ability to capture the seasonal cycle of the HC (Feng et al. 2016b; Feng et al. 2017). Results based on the HadISST and ERSST datasets were similar, and only results based on the ERSST and ERA40 datasets are shown (Figure 9). The response coefficient of the HEA to SEA is much smaller during the cold phase than during warm phase (7.25/4.35/ vs. 18.00/17.37), and the response coefficient of the HES to SES changes little (4.33/2.59 vs. 5.89/3.43) between the warm and cold phases based on the ERSST/HadISST (Table 1). Accordingly, the response contrast of the HC to different SST meridional structures is about 4 (the average of the ERSST and HadISST) during the warm phase, but about 2 during the cold phase. In addition, to the response of the HC to SST but based on the high-pass filter (11-month Gauss filter) during the warm and cold phases is further examined. The regression coefficient of the HEA PC1 (HES PC1) to the SEA PC1 (SES PC1) is 23.90 (6.14) during the warm phase of the IPWP, and it is 6.17 (4.31) for the cold phase based on the ERSST and ERA40 (figure not shown). That is the ratio is 3.9 (1.4) during the warm (cold) phase, and it is 5.5 (1.3) based on the HadISST and ERA40. This further establishes the decreased response contrast of the HEA to SEA under cold IPWP conditions, resulting in a suppressed response contrast of the HC to SST.

In addition to the role El Niño plays in affecting the SST over the IPWP, it has also been reported that SST over the IPWP influences the occurrence of El Niño events (Sun 2003). It has also been noted that a warm Indian ocean may contribute to a weakening of an El Niño event during its development and termination phases (Kug and Kang 2006; Luo et al. 2012). It is thus difficult to distinguish the respective roles of the IPWP and El Niño on basis of the response contrast of the HC to SST. Although multiple reanalyses are available post-1979, the number of warm and cold IPWP events without coincident El Niño events is relatively small. Over longer periods, the available dataset is limited for such a comparison. Therefore, further work will be performed using numerical models to detect the modulation of the IPWP, and the combined modulation of the IPWP and El Niño on the response contrast of the HC to SST.

We have demonstrated that SST meridional distributions within the IPWP have different characteristics between warm and cold events; however, the cause of this difference remains unknown. Previous studies have noted differences in the warming trends between the eastern and western IPWP (e.g., Hu and Hu 2012; Rao et al. 2012; Mathew et al. 2014), and in the zonal gradient of SST within IPWP (Hu and Hu 2012). However, the meridional gradient within the IPWP has received less attention. Our previous work found that the southern and northern IPWP have different warming trends, which could contribute to the formation of the principal mode of the HC (Feng et al. 2013; Li and Feng 2017). In addition, the importance of the meridional gradient of SST on lower-level convergence and vertical circulation has been confirmed in earlier work (Lindzen and Nigam 1987). A further exploration of the cause of the inhomogeneous warming between the southern and northern IPWP will facilitate a better understanding of its impacts on the regional and global circulation and climate.

The focus of this work is the global mean HC; however, the meridional circulation shows strong regional and seasonal characteristics. For example, during the monsoon seasons, the ascending branch of the HC within IPWP can move to 15°N or even farther northward (Li and Zeng 2002; An et al. 2015; Feng et al. 2018). At the same time, the onset of the monsoon causes a strong air–sea feedback within the IPWP. The response of the HC to SST will definitely differ between monsoon and non-monsoon seasons, and between monsoon and non-monsoon regions. Therefore, an exploration of the response of the HC to SST in different regions and different seasons, including the feedbacks of SST on circulation, and a comparison of the differences and similarities that exist in various ocean basins and during different seasons, is required to understand variations of the regional and global HC. Meanwhile, only the situation in the global mean is considered, the HC may be influenced by land conditions as well, therefore, whether the land temperature significantly different during warm and cold IPWP years, and does the HC exhibit significant regional changes away from the open ocean region. These questions are still unresolved and need further work.

In addition, the linear relationship between the HC and tropical SST is investigated, however, previous works have shown that the observed SST-rainfall relationship is highly nonlinear. For example, Gadgil et al. (1984) reported the SST and cloudiness correlated well for the relatively colder oceans, however, the SST ceases to be an important factor in determining the variability of cloudiness when it is above 28°C. Similar SST threshold has been illustrated in Graham and Barnett (1987) but with a value of 27.5°C. And it is indicated that a recent warming of the tropical SST could raise the SST threshold conducive to convection itself (Johnson and Xie 2010). Thefefore, it is of interest to further investigate whether the decreased ratio of the HC to different SST meridional structures during the cold IPWP is related to the reported SST threshold, and to what extent does the SST threshold contribute to the altered ratio.

Finally, knowing the sensitivity of the HC to different SST meridional structures provides a useful method to evaluate the performance of state-of-the-art general circulation models (GCMs), and to assess simulations of the models from phase 5 of the Coupled Model Intercomparison Project (CMIP5). Further work will investigate the capability of the CMIP5 models to reproduce the response contrast of the HC to different SST forcing during warm and cold IPWP conditions, and to predict variations in the HC under future scenarios.

Acknowledgements

This work was jointly supported by the National Natural Science Foundation of China (41705131, 41530424, and 41475076). The HadISST dataset was obtained from the UK Met Office Hadley Centre and is available online at http://www.metoffice.gov.uk/hadobs/hadisst/data/download.html. The NCEP2 and ERSST reanalyses were obtained from NOAA and are available at http://www.esrl.noaa.gov/psd/data/gridded/. The JRA55 reanalysis is available online at http://jra.kishou.go.jp/JRA-55/index_en.html. The ERA40 reanalysis is available online at http://apps.ecmwf.int/datasets/data/era40-moda/levtype=sfc/. The ERAI reanalysis was obtained from http://apps.ecmwf.int/datasets/ .

References

Alory, G., S. Wijffels, G. M. Meyers, 2007: Observed temperature trends in the Indian Oean over 1960-1999 and associated mechanisms. *Geophys. Res. Lett.*, **34**, doi:10.1029/2006GL028044.

An, Z. S., G. X. Wu, J. P. Li, et al., 2015: Global monsoon dynamics and climate change. *Annu. Rev. Earth Planet. Sci.*, **43**, 29-77, doi: 10.1146/annurev-earth-060313-054623.

Cai, W. J., S. Borlace, M. Lengaigne, et al., 2014: Increasing frequency of extreme El Niño events due to greenhouse warming. *Nature Clim. Change*, **4**, 111-116, doi:10.1038/NCIMATE2100.

Cane, M. A., and S. E. Zebiak, 1985: A theory for El Niño and the Southern Oscillation. *Science*, **228**, 1085-1087, doi:10.1126/science.228.4703.1085.

Chang, E. K. M., 1995: The influence of Hadley circulation intensity changes on extratropical climate in an idealized model. *J. Atmos. Sci.*, **52**, 2006-2024.

Dee, D. P., S. M. Uppala, A. J. Simmons, et al., 2011: The ERA-Interim reanalysis: configuration and performance of the data assimilation system. *Q. J. R. Meteorol. Soc.*, **137**(656), 553-597.

Diaz, H. F., and B. Bradley, 2004: The Hadley Circulation: Present, Past and Future. Kluwer Academic Publishers, The Netherlands.

Dong, L., T. J. Zhou, and B. Wu, 2014: Indian Ocean warming during 1958–2004 simulated by a climate system model and its mechanism. *Clim. Dyn.*, **42**, 203-217.

Duan, A. M., C. Sui, and G. X. Wu, 2008: Simulation of local air-sea interaction in the great warm pool and its influence on Asian monsoon. *J. Geophys. Res.*, **113**, D22105, doi:10.1029/2008JD010520.

Feng, J., and J. P. Li, 2011: Influence of El Niño Modoki on spring rainfall over south China. *J. Geophys., Res.*, **116**, D13102, doi: 10.1029/2010JD015160.

Feng, J., J. P. Li, and F. Xie, 2013: Long-term variation of the principal mode of boreal spring Hadley circulation linked to SST over the Indo-Pacific warm pool. *J. Climate*, **26**, 532-544.

Feng, J., and J. P. Li, 2013: Contrasting impacts of two types of ENSO on the boreal spring Hadley circulation. *J. Climate*, **26**, 4773-4789.

Feng, J., J. P. Li, F. F. Jin, et al., 2016a: Contrasting responses of the Hadley circulation to equatorially asymmetric and symmetric meridional sea surface temperature structures. *J. Climate*, **29**, 8949-8963.

Feng, J., Jianlei Zhu, and F. Li, 2016b: Climatological vertical features of Hadley circulation depicted by the NCEP/NCAR, ERA40, NCEP-DOE, JRA25, ERA-Interim, and CFSR reanalyses. *SOLA*, **12**, 237-241, doi: 10.2151/sola.2016-047.

Feng, J., J. P. Li, F. F. Jin, et al., 2017: The responses of the Hadley circulation to different meridional SST structures in the seasonal cycle. *J. Geophys. Res.*, **122**, 7785-7799, doi:10.1002/2017JD026953.

Feng, J., J. P. Li, F. F. Jin, et al., 2018: Relationship between the Hadley circulation and different tropical meridional SST structures during boreal summer. *J.*

Climate, **31**, 6575-6590.

Feng, R., J. P. Li, and J. C. Wang, 2011: Regime change of the boreal summer Hadley circulation and its connection with the tropical SST. *J. Climate*, **24**, 3867-3877.

Gadgil, S., P. V. Joseph, and N. V. Joshi, 1984: Ocean-atmosphere coupling over monsoon regions. *Nature*, **312**, 141-143.

Graham, N. E., and T. P. Barnett, 1987: Sea surface temperature, surface wind divergence, and convection over tropical oceans. *Science*, **238**, 657-659.

Hu, S. J., and D. X. Hu, 2013: Review on the western Pacific warm pool study. *Studia Marina Sinica*, **51**, 37-48.

Johnson, N. C., and S. P. Xie, 2010: Changes in the sea surface temperature threshold for tropical convection. *Nat. Geosci.*, **3**, 842-845.

Kanamitsu, M., W. Ebisuzaki, J. Woollen, et al., 2002: NCEP-DOE AMIP-II Reanalysis (R-2). *Bull. Amer. Meteorol. Soc.*, **83**, 1631-1643.

Kidwell, A., L, Han, Y. H. Jo, and X. H. Yan, 2015: Decadal western Pacific warm pool variability: A centroid and heat content study. *Sci. Rep.*, **7**, 13141, doi:10.1038/s41598-017-13351-x.

Kobayashi, S., Y. Ota, Y. Harada, et al., 2015: The JRA-55 reanalysis: General specifications and basic characteristics. *J. Meteor. Soc. Jap.*, **93**(1), 5-48.

Kug, J. S., and I. S. Kang, 2006: Interactive feedback between ENSO and the Indian Ocean. *J. Climate*, **19**, 1784-1801.

Lau, N. C., and M. J. Nath, 2003: Atmosphere–ocean variations in the Indo-Pacific sector during ENSO episodes. *J. Climate*, **16**, 3-20.

Li, J. P., and Q. C. Zeng, 2002: A unified monsoon index. *Geophys. Res. Lett.*, **29**(8), 1274, doi:10.1029/2001GL013874.

Li, J. P., R. C. Ren, Y. Q. Qi, et al., 2013: Progress in air-land-sea interactions in Asia and their role in global and Asian climate change. *Chinese Journal of Atmospheric Sciences* (in Chinese), **37**(2), 518-538.

Li, J. P., and J. Feng, 2017: Tropical large-scale atmospheric interaction in association with subtropical aridity trend. Aridity trend in Northern China, Fu CB, Mao HT Eds, World Scientific Publishing Co Pte Ltd, 320pp.

Lindzen, R. S., and S. Nigam, 1987: On the role of sea surface temperature gradients in forcing low-level winds and convergence in the tropics. *J. Atmos. Sci.*, **44**, 2418-2436.

Lindzen, R. S., 1994: Climate dynamics and global change. *Annu. Rev. Fluid Mech.*, **26**, 353-378.

Lo, L., C. C. Shen, K. Y. Wei, et al., 2014: Millennial meridional dynamics of the Indo-Pacific warm pool during the last termination. *Clim. Past*, **10**, 2253-2261.

Luo, J.-J., W. Sasaki, Y. Masumoto, 2012: Indian Ocean warming modulates Pacific climate change. *Proc. Natl. Acad. Sci. U.S.A.*, **109**, 18701–18706.

Ma, J., and J. P. Li, 2008: The principal modes of variability of the boreal winter Hadley cell. *Geophys. Res. Lett.*, **35**, L01808, doi:10.1029/2007GL031883.

Mathew, K. R., K. Ritika, P. Terray, et al., 2014: The curious case of Indian Ocean warming. *J. Climate*, **27**, 8501-8509.

Numaguti, A., 1994: Dynamics and energy balance of the Hadley circulation and the tropical precipitaton zones, Part II: sensitivity to meridional SST distribution. *J. Atmos. Sci.*, **52**, 1128-1141.

Quan, X., H. F. Diaz, and M. P. Hoerling, 2002: The conference on the Hadley circulation: Present, Past and Future, November 12-15, 2002, Honolulu, Hawaii.

Rayner, N. A., and Co-authors, 2003: Global analyses of sea surface temperature, sea ice, and night marine air temperature since the late nineteenth century. *J. Geophys. Res.*, **104**, D14, 4407, doi: 10.1029/2002JD002670.

Rao, S. A., A. R. Dhakate, S. K. Saha, et al., 2012: Why is Indian Ocean warming consistently? *Clim. Change*, **110**, 709-719.

Roxy M. K., K. Ritika, P. Terray, and S. Masson, 2014: The curious case of Indian Ocean warming. *J. Climate*, **27**, 8501-8509.

Rind, D., and W. B. Rossow, 1984: The effects of physical processes on the Hadley circulation. *J. Atmos. Sci.*, **41**, 479-507.

Santoso, A., M. J. Mcphaden, and W. J. Cai, 2017: The defining characteristics of ENSO extremes and the strong 2015/2016 El Niño. *Rev. Geophys.*, **55**, 1079-1129.

Sardeshmukh, P. D., B. J. Hoskins, 1988: The generation of global rotational flow by steady idealized tropical divergence. *J. Atmos. Sci.*, **45**, 1228-1251.

Schneider, E., and R. S. Lindzen, 1977: Axially symmetric steady state models of the basic state of instability and climate studies. Part I: Linearized calculations. *J. Atmos. Sci.*, **34**, 253-279.

Smith, T. M., R. W. Reynolds, T. C. Peterson, and J. Lawrimore, 2008: Improvements to NOAA's historical merged land-ocean surface temperature analysis (1880-2006). *J. Climate*, **21**, 2283-2296.

Swapna, P., R. Krishnan, and J. M. Wallace, 2014: Indian Ocean and monsoon coupled interactions in a warming environment. *Clim. Dyn.*, **42**, 2439-2454.

Uppala, S. M., P. W. Kallberg, A. J. Simmons, et al., 2005: The ERA-40 reanalysis. *Q. J. R. Meteor. Soc.*, **131**, 2961-3012.

Webster, P. J., R. Lukas, 1992: TOGA COARE: The coupled ocean atmosphere response experiment. *Bull. Amer. Meteorol. Soc.*, **73**, 1377-1416.

Williams, A. P., and C. Funk, 2011: A westward extension of the warm pool leads to a westward extension of the Walker circulation, drying eastern Africa. *Clim. Dyn.*, **37**, 2417-2435.

Waliser, D. E., A. Shi, J. R. Lanzante, and A. H. Oort, 1999: The Hadley circulation: assessing NCEP/NCAR reanalysis and sparse in-situ estimates. *Clim. Dyn.*, **15**, 719-735.

Xiao, D., and J. P. Li, 2011: Mechanism of stratospheric decadal abrupt cooling in the early 1990s as influenced by the Pinatubo eruption. *Chin. Sci. Bull.*, **56**, 772-780, doi: 10.1007/s11434-010-4287-9.

Xie, S. P., H. M. Xu, W. S. Kessler, and M. Nonaka, 2005: Air-sea interaction over the eastern Pacific warm pool: gap winds, thermocline dome, and atmospheric convection. *J. Climate*, **18**, 5-20.

Xie, S. P., K. M. Hu, J. Hafner, et al., 2009: Indian ocean capacitor effect on Indo-Western Pacific climate during the summer following El Niño. *J. Climate*,

22, 730-747.

Yan, X. H., C. R. Ho, Q., Zheng, and V. Klemas, 1992: Temperature and size variabilities of the Western Pacific Warm Pool. *Science*, **258**, 1643-1645.

Zhang, L., W. Q. Han, and F. Sienz, 2018: Unraveling causes for the changing behavior of tropical Indian Ocean in the past few decades. *J. Climate*, **31**(6), 2377-2388.

Table 1. Regression coefficients between the HEA (HES) PC1 with respect to the SEA (SES) PC1and their ratio calculated using the various reanalysis datasets.

Types	Dataset	ERSST			HadISST		
		ASY	SYM	Ratio	ASY	SYM	Ratio
Warm events	JRA	82.78	14.09	5.9	44.29	8.99	4.9
	NCEP2	35.17	7.06	5.0	20.59	4.36	4.7
Cold events	JRA	28.72	14.50	2.0	12.34	9.34	1.3
	NCEP2	14.09	7.82	1.8	5.63	5.26	1.1
Warm phase	ERA40	18.00	5.89	3.1	17.37	3.43	5.1
Cold phase	ERA40	7.25	4.33	2.0	4.35	2.59	1.7

Figure Captions:

Figure 1. (a) The EOF1 of the monthly HC based on JRA (contour), and the climatological distribution of the HEA (shaded) during the warm IPWP events. The contour interval is 0.03×10^{10} kg/s. Solid (dotted) contours are positive (negative) and the zero contour is thickened. (b)-(c) As in (a), but based on the NCEP2 and ERAI, respectively. Right panel, As in the left, but for the HES.

Figure 2. As in Figure 1, but for the distribution during the cold IPWP events.

Figure 3. (a) The EOF1 of the SEA during the warm IPWP events, (b) As in (a), but for the SES. (c)-(d) As in (a)-(b), but for the distributions during the cold IPWP events. The red and blue lines indicate based on the ERSST and HadISST datasets, respectively.

Figure 4. (a) Scatter plot of the PC1s of the SEA against the PC1s of the HEA during the warm events (circles), and their linear fit (red squares). (b) As in (a), but for the scatter plot of the PC1s of the SES against the PC1s of the HES. (c)-(d) As in (a)-(b), but during the cold events.

Figure 5. Composite SST anomalies during the (a) warm, and (b) cold IPWP events. (c) Sum of the SST anomalies during the warm and cold events. Contour lines indicate the 0.05 significance level.

Figure 6. Profiles of SST anomaly averaged over the IPWP during the (a) warm, (b) cold, and (c) sum of the warm and cold events (°C). The red and blue lines indicate based on the ERSST and HadISST datasets, respectively.

Figure 7. Regression pattern of the MSF (shaded) and vertical motion (contour) with

respect to the MSGI.

Figure 8. (a) Seasonal cycle of the areal mean SST anomalies within north Pacific (30°-50°N, 140°E-130°W) in the warm (red) and cold (blue) events based on the ERSST. (b) As in (a), but based on the HadISST.

Figure 9. As in Figure 4, but for the result during the (upper) warm 1997-2001 and (below) cold phases 1958-1972 of the IPWP.

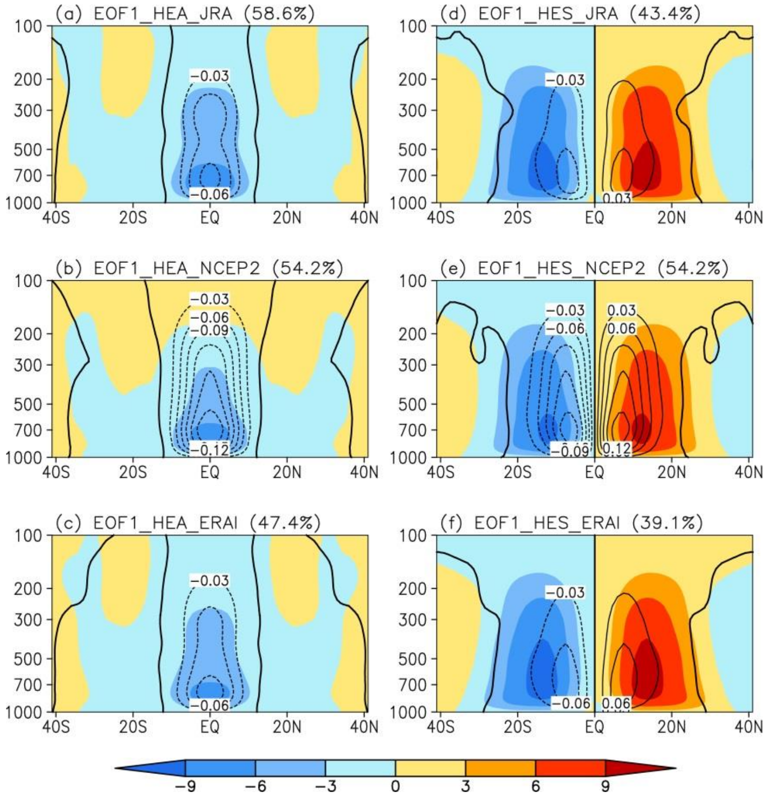

Figure 1. (a) The EOF1 of the monthly HC based on JRA (contour), and the climatological distribution of the HEA (shaded) during the warm IPWP events. The contour interval is 0.03×10^{10} kg/s. Solid (dotted) contours are positive (negative) and the zero contour is thickened. (b)-(c) As in (a), but based on the NCEP2 and ERAI, respectively. Right panel, As in the left, but for the HES.

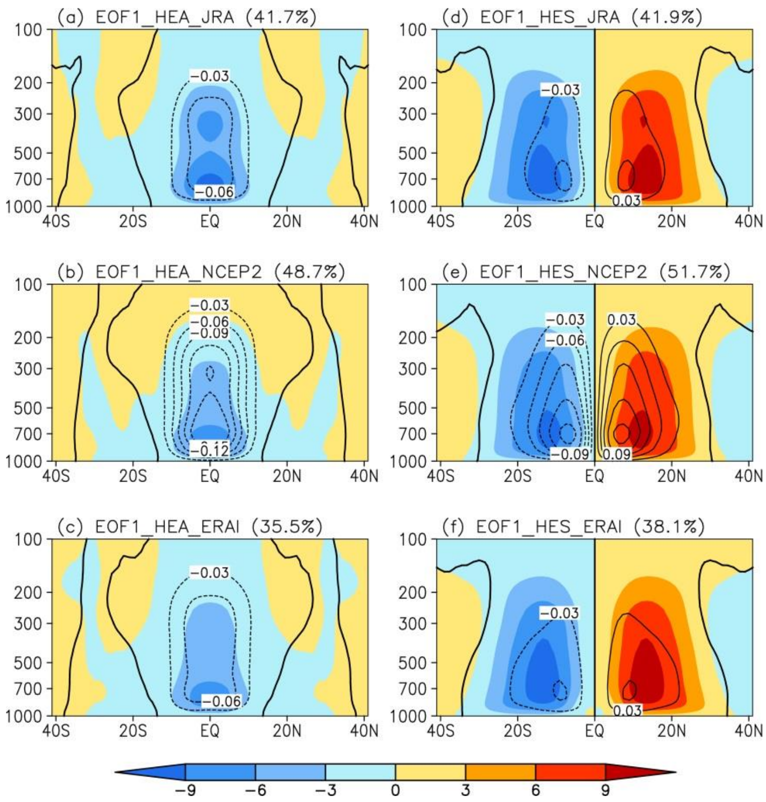

Figure 2. As in Figure 1, but for the distribution during the cold IPWP events.

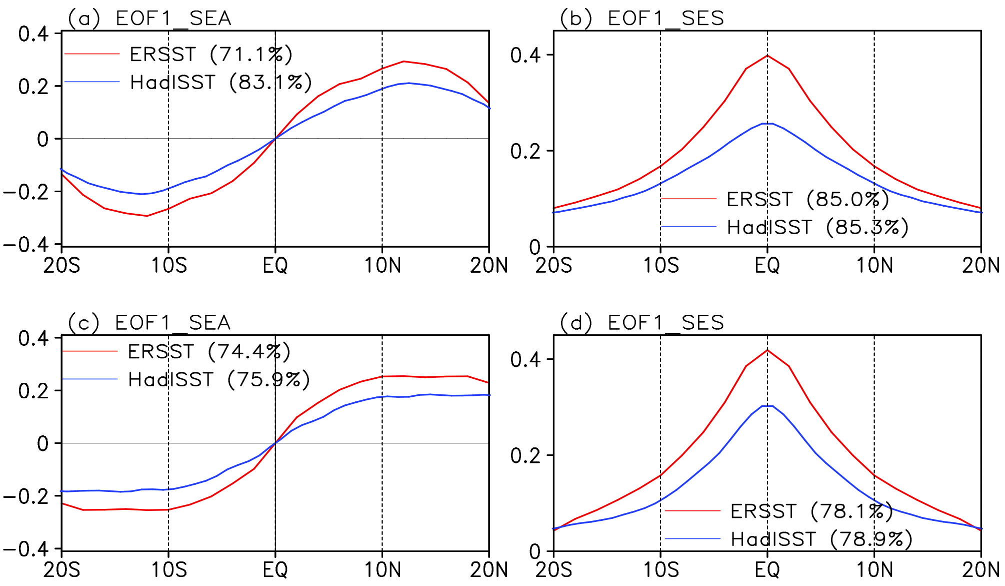

Figure 3. (a) The EOF1 of the SEA during the warm IPWP events, (b) As in (a), but for the SES. (c)-(d) As in (a)-(b), but for the distributions during the cold IPWP events. The red and blue lines indicate based on the ERSST and HadISST datasets, respectively.

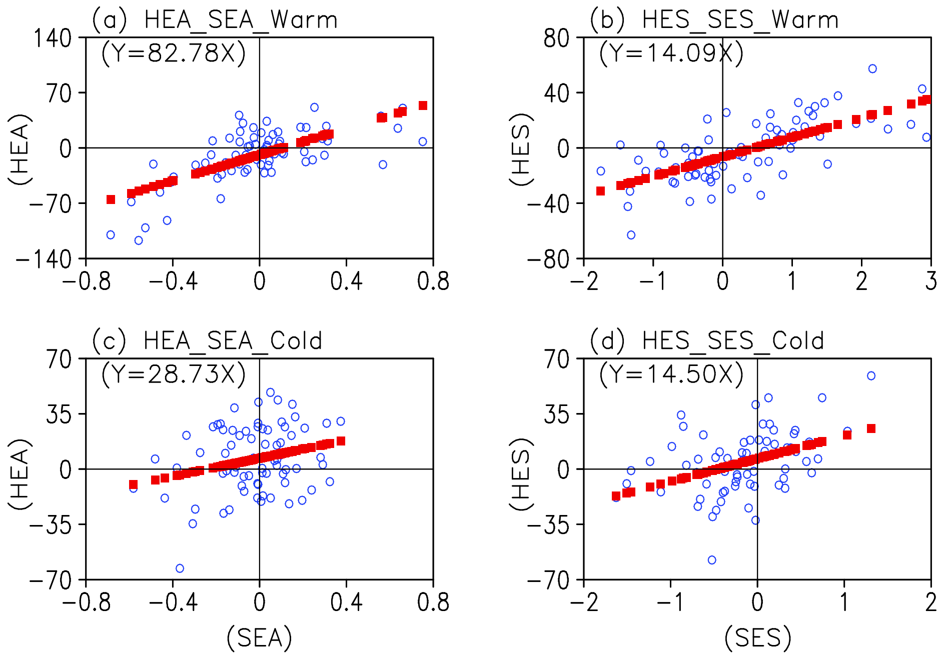

Figure 4. (a) Scatter plot of the PC1s of the SEA against the PC1s of the HEA during the warm events (circles), and their linear fit (red squares). (b) As in (a), but for the scatter plot of the PC1s of the SES against the PC1s of the HES. (c)-(d) As in (a)-(b), but during the cold events.

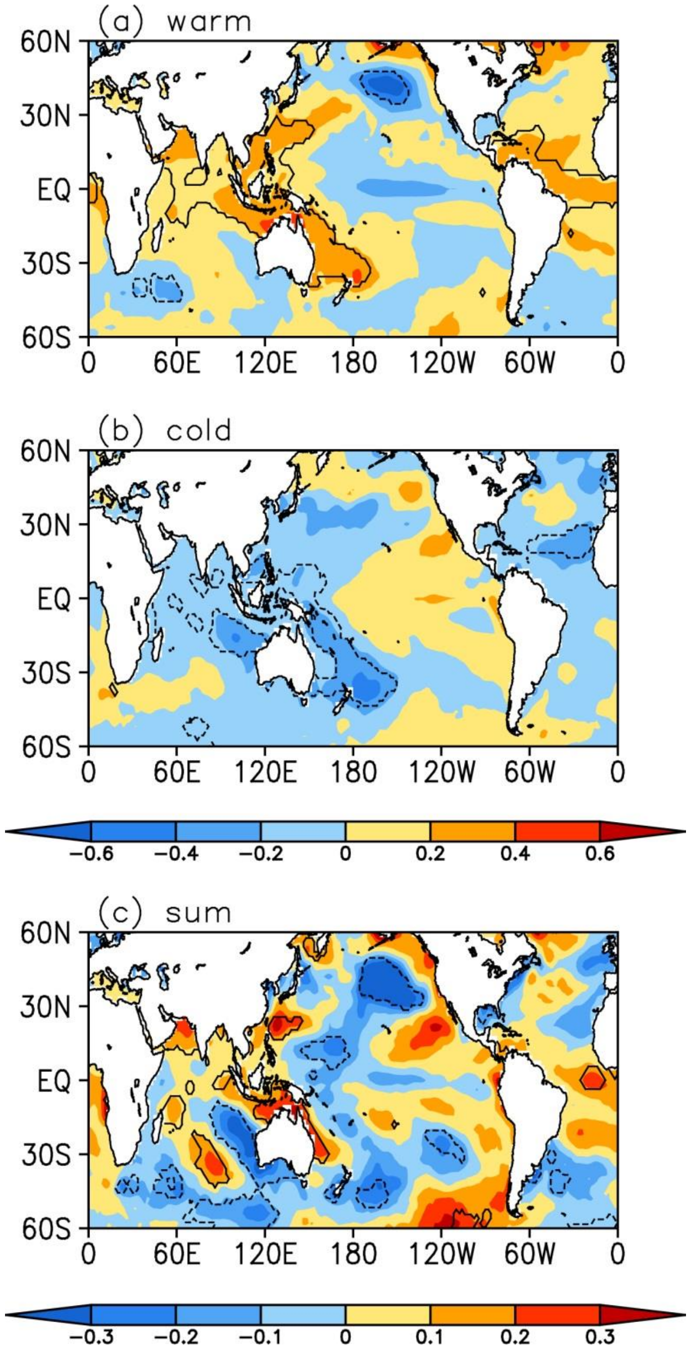

Figure 5. Composite SST anomalies during the (a) warm, and (b) cold IPWP events. (c) Sum of the SST anomalies during the warm and cold events. Contour lines indicate the 0.05 significance level.

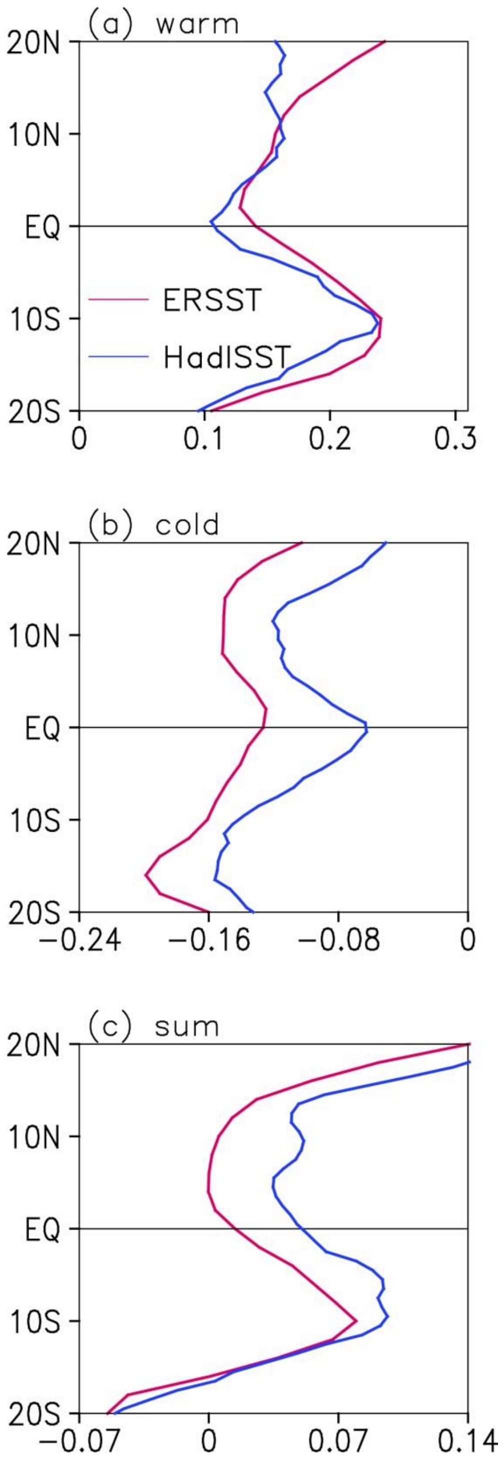

Figure 6. Profiles of SST anomaly averaged over the IPWP during the (a) warm, (b) cold, and (c) sum of the warm and cold events (°C). The red and blue lines indicate based on the ERSST and HadISST datasets, respectively.

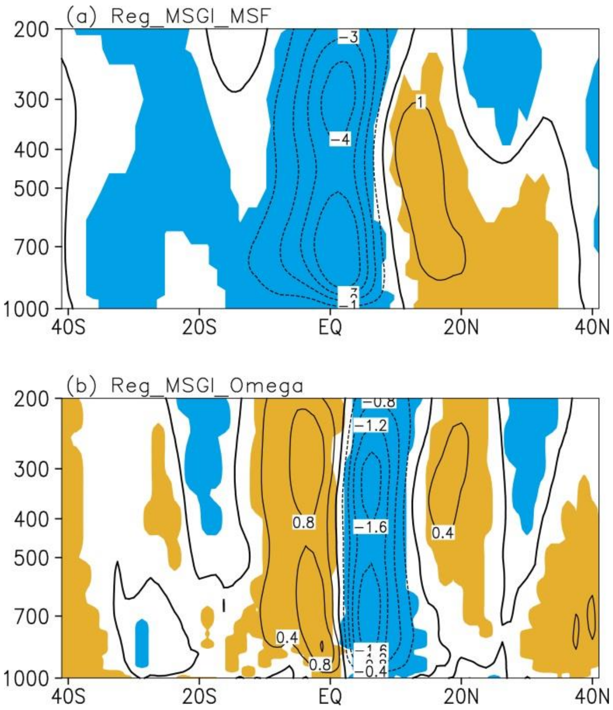

Figure 7. Regression pattern of the (a) MSF and (b) vertical motion with respect to the MSGI. Shading indicates the 0.05 significance level.

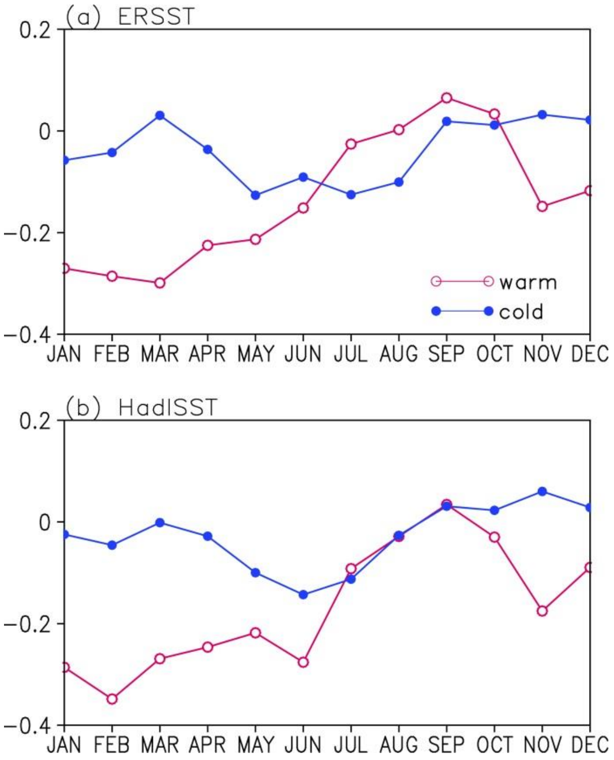

Figure 8. (a) Seasonal cycle of the areal mean SST anomalies within north Pacific (30°-50°N, 140°E-130°W) in the warm (red) and cold (blue) events based on the ERSST. (b) As in (a), but based on the HadISST.

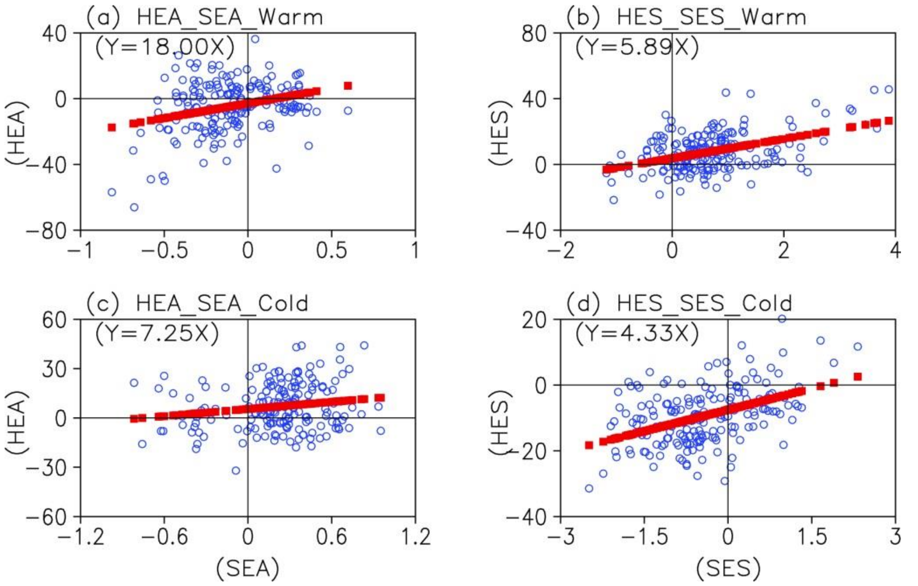

Figure 9. As in Figure 4, but for the result during the (upper) warm 1997-2001 and (below) cold phases 1958-1972 of the IPWP.